



Supplementary Information for

Commercial AHAS inhibiting herbicides are promising drug leads for the treatment of human fungal pathogenic infections.

Mario D. Garcia, Sheena M. H. Chua, Yu-Shang Low, Yu-Ting Lee, Kylie Agnew-Francis, Jian-Guo Wang, Amanda Nouwens, Thierry Lonhienne, Craig M. Williams, James A. Fraser, Luke W. Guddat*

*Correspondence should be addressed to L.W.G. (e-mail: luke.guddat@uq.edu.au)

This PDF file includes:

Supplementary text

Figures S1 to S10

Tables S1 and S2

References

Supplementary text

Detailed herbicide binding mode to CaAHAS

Binding mode of the SUs. The scaffold of the SUs comprises an aromatic ring (R) and a pyrimidine or triazine ring (R') linked by a sulfonylurea bridge (R-SO₂-NH-CO-NH-R') (**Figure S1**). The SUs form up to five polar contacts with R376 and K247 and >30 non-polar interactions with twelve residues of the CaAHAS herbicide-binding pocket and with FAD. To illustrate, in the CaAHAS-CE complex (**Figure 4a**) the guanidino group of R376 forms four hydrogen bonds with CE, two of these with the carbonyl oxygen of the urea bridge and the other two with the methoxy oxygen and a nitrogen atom of the pyrimidine ring. A fifth hydrogen bond is formed between the amino group of K247 and the nitrogen atom adjacent to the sulfonyl group of CE, which is expected to be deprotonated (pK_a 4.2) at physiological pH and at the pH of co-crystallization. In addition, CE forms a large number of non-polar interactions with eleven residues of the herbicide-binding site (**Figure S7**). The majority of these contacts are with the highly conserved residues F197, M350, M578, and W582, all located in the deepest part of the binding pocket (**Figure S2b**). Indeed, the side-chain of W582 is a major contributor to binding by forming π stacking interactions with the heterocyclic ring of the herbicide (**Figure 4a and S7**). Non-polar interactions with P188 and D375, both located at the entrance of the access channel, induce a bent conformation in CE and the other SUs (**Figure 4a**) as has been observed when the SUs bind AtAHAS (1). This conformation allows the establishment of a π cation interaction between the aromatic ring and the guanidinium group of R376 (**Figure S7**).

An overlay of the five CaAHAS-SU complexes shows that the side chain positions of the residues in the herbicide-binding site do not change significantly when different SUs are bound. However, the conformation of the SU herbicides changes depending on the different attachments to the aromatic and heterocyclic rings (**Figure S8a and b**). Given that CE, SM, IE and IM possess the general scaffold of the SUs ($R-SO_2-NH-CO-NH-R'$), these inhibitors adopt similar conformations in CaAHAS. On the other hand, BSM has an extra carbon atom between the aromatic ring and the sulfonyl group ($R-CH_2-SO_2-NH-CO-NH-R'$), implying that more space is required to accommodate this extra atom. As a result, the sulfonyl group in BSM shifts its position 1.24 Å towards R376. In addition, there is a 180° rotation around the NH-CO-NH bonds of the urea bridge that induces an S-shaped sulfonylurea bridge rather than the U-shaped bridge observed for the other SUs (**Figure S8b**). Furthermore, when BSM is bound, the heterocyclic ring inserts deeper into the herbicide-binding site (0.44 - 0.73 Å closer to the C2 atom of ThDP) and is oriented more towards FAD than other SUs.

Binding mode of the TPs. TPs are composed of aromatic (R) and triazolopyrimidine (R') rings linked together by a sulfonamide bridge (**Figure S1**). In the CaAHAS-MT complex, the guanidinium group of R376 forms hydrogen bonds with the N1 atom of the triazole ring and with a sulfonyl oxygen atom of the linker. Two additional hydrogen bonds are formed between the amino group of K247, a sulfonyl oxygen atom and the deprotonated amino group (pK_a 5.5) of the linker in the herbicide. W582 forms a π stacking interaction with the heterocyclic ring, locking this moiety deepest in the herbicide-binding site (**Figure**

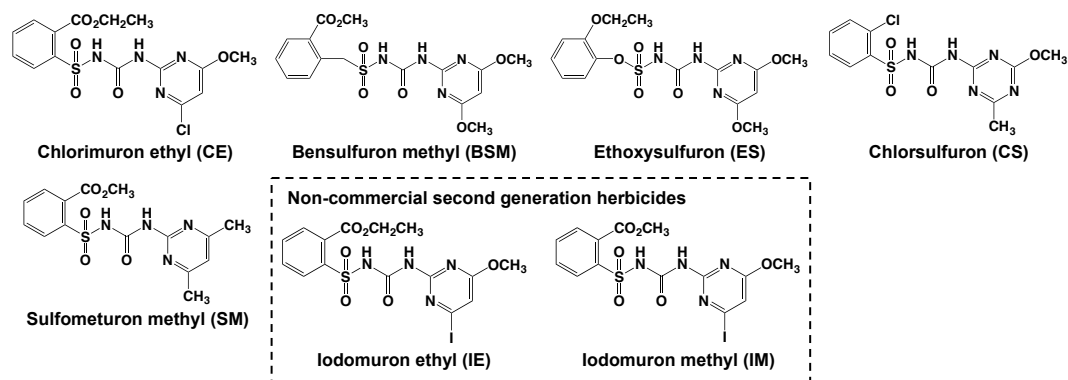
4b). Only ten additional residues assist in herbicide binding (**Figure S7**); however, MT has the lowest K_i value amongst all herbicides tested against CaAHAS (**Table 1**). In the CaAHAS-PS complex, K247 forms a salt bridge with the nitrogen atom of the sulfonamide linker, also expected to be deprotonated at most physiological pH values and at the pH of crystallization (pK_a 5.1). Five additional hydrogen bonds involve the guanidium group of R376, the difluoroethoxy oxygen and fluorine atoms attached to the aromatic ring, a sulfonyl oxygen of the linker, the N1 atom of the triazole ring and one of the methoxy oxygen atoms of the dimethoxy-triazolopyrimidine ring (**Figure S7**). In addition, PS forms a number of hydrophobic and van der Waals interactions with fourteen residues of the herbicide-binding site, including the π stacking interaction with W582. It is worth noting that the orientation of the sulfonamide bridge in MT and PS is different. While in MT (and the majority of the TPs) the amide group is adjacent to the aromatic ring and the sulfonyl group is adjacent to the heterocyclic ring ($R-NH-SO_2-R'$), in PS the position of these groups is reversed ($R-SO_2-NH-R'$). As a result, when the MT and PS complexes are superposed, the side chain of W582 rotates $\sim 163^\circ$ around the Cy atom to accommodate MT and to avoid forming steric clashes with the oxygen atoms of the sulfonyl group (**Figure S8c**). Another significant difference is the position of the sulfonyl group in the two complexes, which is displaced by 1.24 Å (**Figure S8a and c**). Consequently, the angle that the plane of their heterocyclic rings makes when binding to the pocket varies by $\sim 20^\circ$.

Binding mode of the SCTs. The SCTs comprise a triazolinone ring, a sulfonylamido linker, and an aromatic ring. PC binds to CaAHAS with the

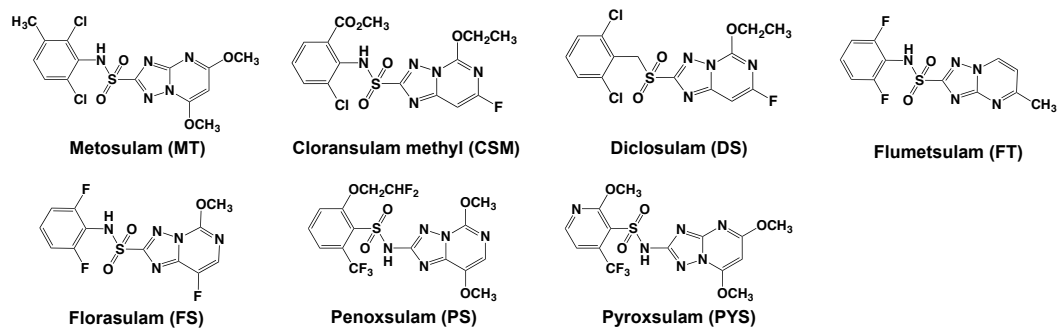
triazolinone moiety inserted deepest in the herbicide-binding site, forming a π stacking interaction with W582 (**Figure 4c**). The carbonyl substituent and the N2 atom at this position are within hydrogen bonding distance of the amino terminal groups of K247 and R376. The propoxy substituent inserts in the cavity formed between the isoalloxazine ring of FAD and the side chains of F197, R376 and M350, and M578. The linker extends along the binding pocket with the exposed amino group ($pK_a = 2.1$) and the carbonyl oxygen forming hydrogen bonds with K247 and R376, respectively. Like the SUs, the monosubstituted aromatic moiety of PC adopts a bent conformation induced by non-polar interactions with P188 and D375. In total, PC interacts with twelve residues and with FAD, resulting in >40 non-covalent interactions.

Supplementary figures

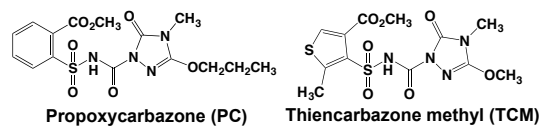
Sulfonylureas



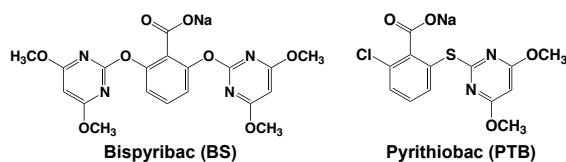
Triazolopyrimidines



Sulfonylamino-carbonyl-triazolinones



Pyrimidinyl-benzoates



Imidazolinones

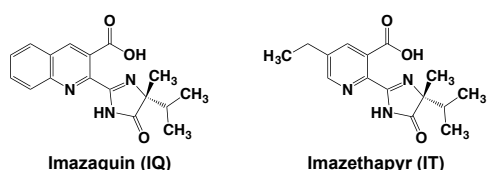


Figure S1. Chemical structures of the AHAS inhibitors evaluated in this study.

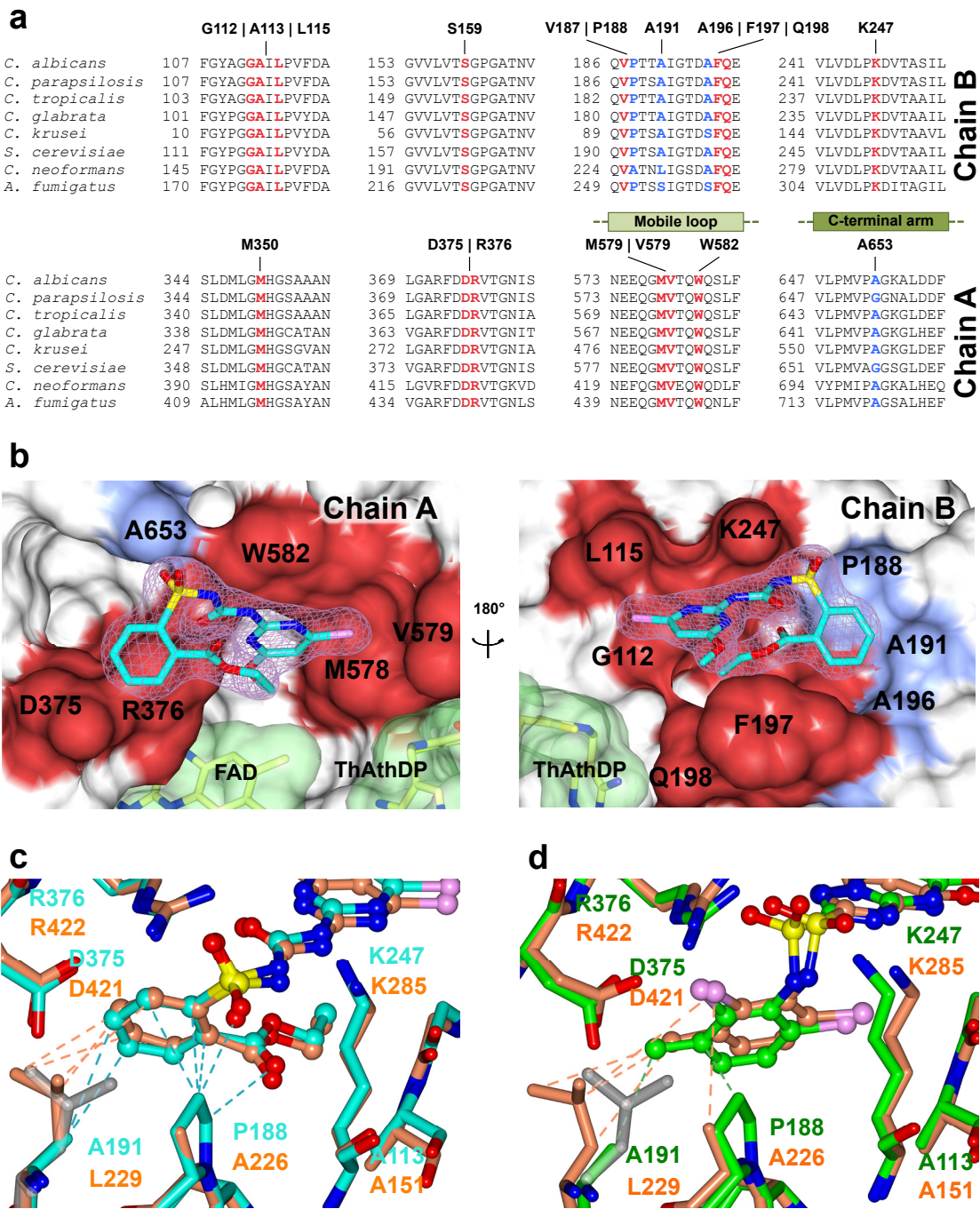


Figure S2. Residues contouring the herbicide-binding pocket in fungal AHASs. **a** Multiple sequence alignment of the loops involved in herbicide binging in eight fungal AHASs. Highly conserved residues of the herbicide-binding site are coloured red, whereas conserved residues are blue. Other residues not forming interactions with the herbicides are depicted black. **b** Surface representation showing the position of CE in the herbicide-binding site of

CaAHAS. The herbicide, and the enzyme cofactors, FAD and ThDP, are depicted as stick models with carbon coloured cyan and light yellow, respectively. CE is superposed onto the F_o - F_c omit electron density map contoured to 3.5 σ . The surface for FAD and ThDP is in light green. The residues forming interactions with the herbicide are coloured as per panel a. **c, d** Computational models of the P188A and A191L substitutions, present in CnAHAS, performed in the crystal structures of CaAHAS in complex with (c) CE or (d) MT. The inhibitors are shown in ball and stick models and the residues of the herbicide-binding site in stick models. The CnAHAS-CE/MT models are orange; the CaAHAS-CE complex, cyan; and the CaAHAS-MT complex, green. L229 shown in gray transparency represents the conformation adopted by this residue when the mutation A191L was modelled in uninhibited CaAHAS. Broken lines represent non-polar interactions observed after energy minimization using Yasara (2).

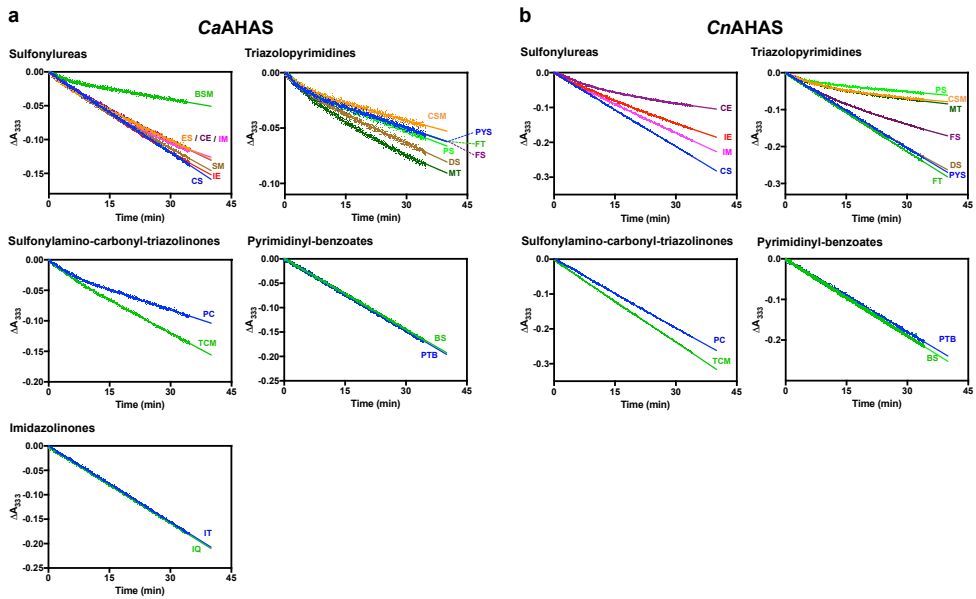


Figure S3. Progress curves for the inhibition of 1 μM enzyme by different herbicide families. The inhibition of **a** 1 μM CaAHAS or **b** 1 μM CnAHAS was measured in the presence of representatives of the five families of AHAS inhibiting herbicides. The inhibitor concentration varied depending on the enzyme tested. For CnAHAS, all inhibitors were assayed at a concentration of 100 nM. For CaAHAS, the inhibitor concentrations were CE (25 nM), ES (40 nM), IM (25 nM), IE (25 nM), MT (10 nM), PS (12.5 nM), FS (31.25 nM), DS and CSM (30 nM), and BSM, SM, CS, PYS, FT, PCS, TCM, BS, PTB, IQ and IT (100 nM). The experimental data was fitted using Eq. 3 (3) (solid lines) giving the first order rates of enzyme inactivation (k_{iapp}) and enzyme recovery (k_3) for each herbicide. The effective ratio of free enzyme/enzyme-inhibitor complex (F value) for FT, PC, PYS, SM and TCM, for CaAHAS, and BS, CS, DS, FS, FT, IM, PC, PS, PTB, PYS, and TCM, for CnAHAS, was calculated according to the inhibititon constant formula (Eq. 4) taking into account the low affinity of these herbicides for the enzyme (see Materials and Methods). Note that BS, CS, IQ, IT and PTB do not show accumulative inhibition of CaAHAS. A similar situation is observed for BS, CS, PTB and TCM when inhibiting CnAHAS.

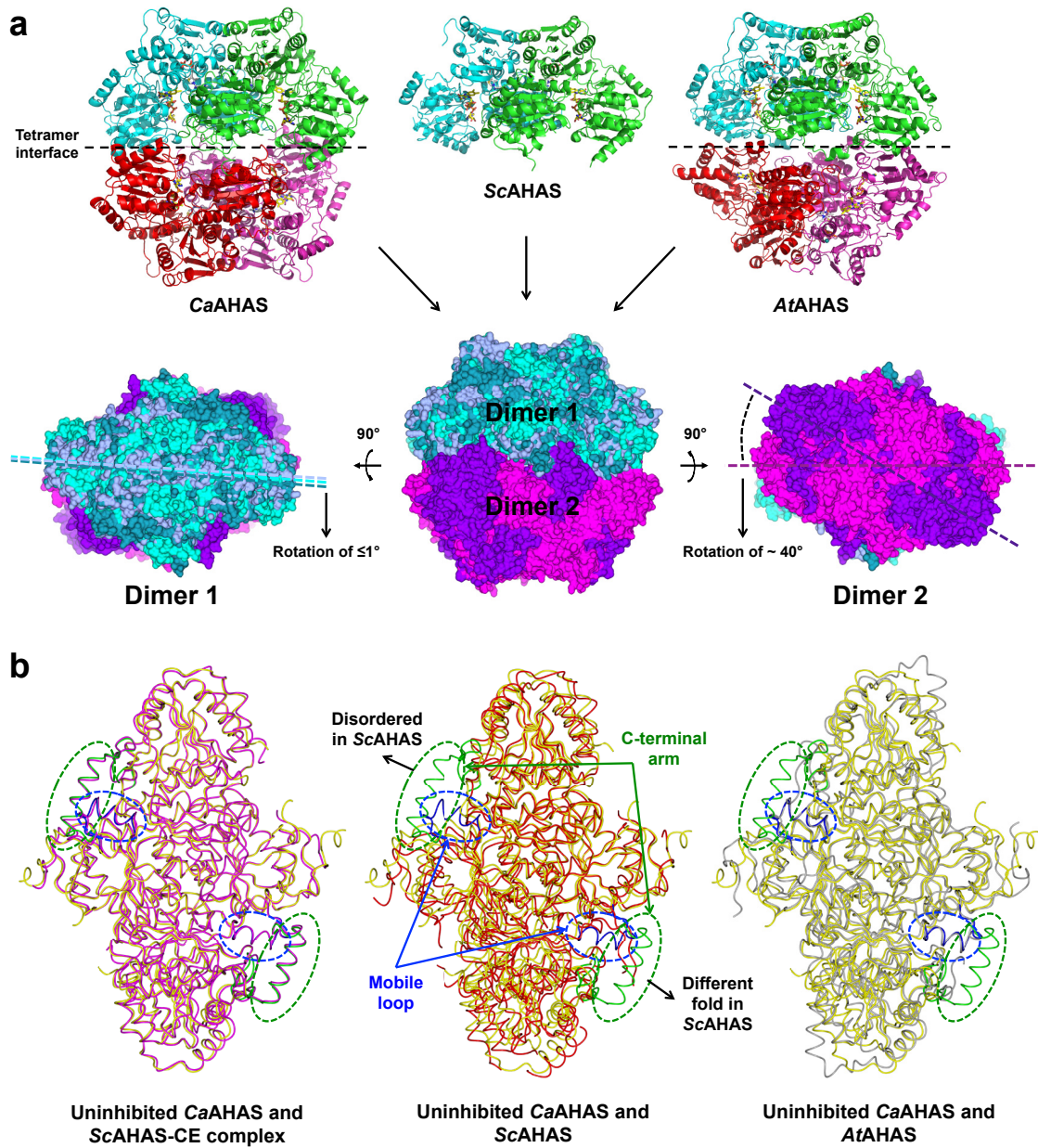


Figure S4. Overall structures of AHASs form *A. thaliana*, *S. cerevisiae* and *C. albicans*. **a** Cartoon representation of the AtAHAS (homotetramer; PDB code 5K6Q) ScAHAS (homodimer; PDB code 1JSC) and CaAHAS (homotetramer) structures (Upper panel). CaAHAS has an overall fold similar to ScAHAS, but is tetrameric rather than dimeric. In this way, it adopts an oligomerization state that resembles plant AHAS. The polypeptide in each subunit is coloured differently. The enzyme cofactors FAD and ThDP are shown as yellow stick models, and the Mg²⁺ ion is shown as a dark cyan sphere. The lower panel shows surface

representations of the superposition of *AtAHAS*, *ScAHAS* and *CaAHAS* in three different views. The *ScAHAS* dimer (light blue) and dimer 1 of *AtAHAS* (cyan) and *CaAHAS* (dark cyan) are superimposable (rmsd = 0.48 to 1.01 Å), having similar orientations (represented with broken lines; ~1° of difference). In contrast, the second dimer of *AtAHAS* (magenta) and *CaAHAS* (purple) are orientated differently (represented with broken lines). Relative to *AtAHAS*, in *CaAHAS* there is a rotation of ~40° around the tetramer interface. **b** Worm representation of uninhibited *CaAHAS* (yellow), *ScAHAS* (1JSC, red) and *AtAHAS* (5K6Q, gray) and *ScAHAS* in complex with CE (1N0H, magenta). Superposition of these structures shows the capping region (mobile loop, blue; and C-terminal arm, green) in *CaAHAS* is ordered, similarly to both *ScAHAS* in complex with herbicide and uninhibited *AtAHAS*. The capping region in free *ScAHAS* is disordered or has a different fold. The overall fold of *CaAHAS* is similar to *ScAHAS* when bound to herbicide.

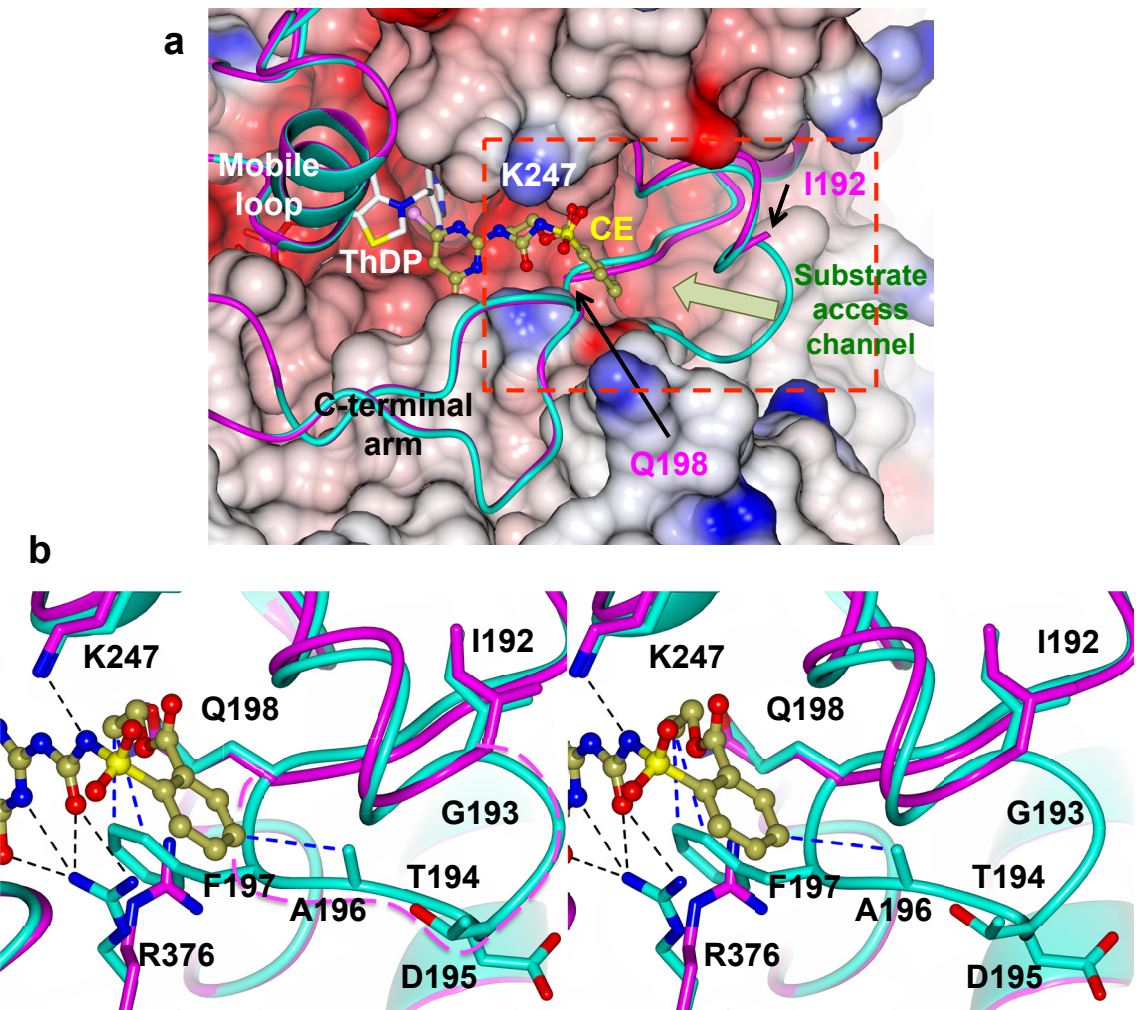


Figure S5. Herbicide binding pocket in CaAHAS. **a** Electrostatic potential surface representation of the active site, herbicide-binding site and substrate access channel (enclosed with broken lines) in the CaAHAS-CE complex showing the mobile loop (Q576-Y591), the C-terminal arm (P646-Y683) and the P188-D201 region in cartoon representations. The herbicide-binding site and substrate access channel in the CaAHAS-CE complex (cyan) were superposed onto the corresponding regions in the uninhibited CaAHAS structure (magenta). Note the residues between I192 and Q198 (indicated with black arrows) are disordered in the uninhibited enzyme. CE (gold ball and stick models) binds at the entrance of the active site, where ThDP (white sticks) is located, and inhibits the enzyme activity by blocking substrate access. **b** Stereoview of the

enclosed section in panel a. In the uninhibited CaAHAS structure, the residues between I192-Q198 are disordered (magenta dashed line), and the side chain of R376 partially occupies the position adopted by the aromatic ring of F197 when an inhibitor is bound. In the presence of an herbicide, such as CE, the residues between I192-Q198 become ordered due to a number non-covalent interactions formed between the herbicide and A196, F197 and Q198 (blue broken lines). The side chain of R376 changes its orientation due to the formation of four hydrogen bonds with the herbicide (black broken lines). The observed flexibility of R376 and the I192-Q198 loop may be necessary to facilitate substrate access.

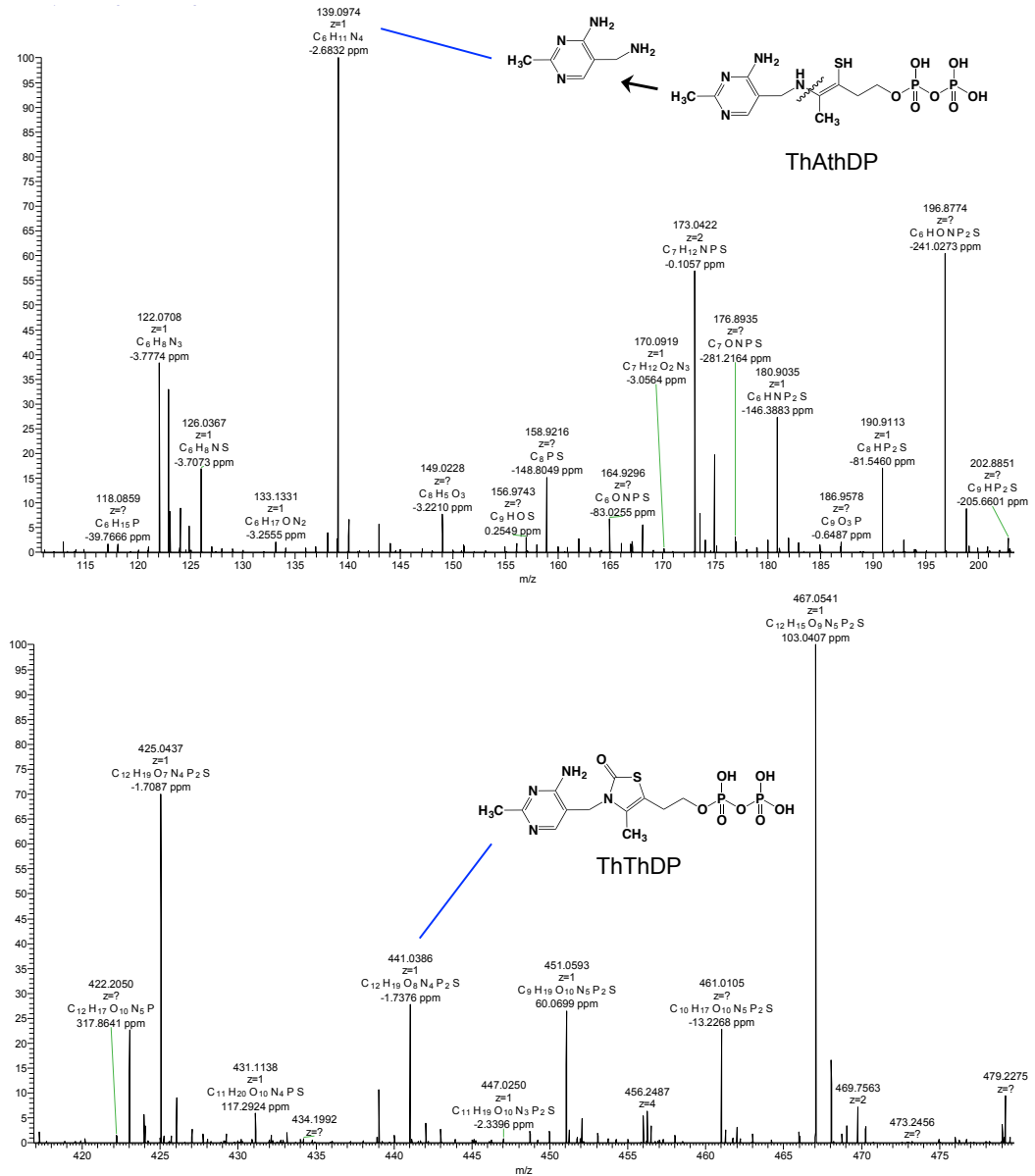


Figure S6. High-resolution mass spectrometry data of ThDP. ThDP was isolated from CaAHAS incubated with inhibitor (CE, MT, PS or PC) and analyzed by LC-MS. A fragment of ThAthDP (molecular formula $\text{C}_6\text{H}_{10}\text{N}_4$; calculated $[\text{M}+\text{H}]^+$ of 139.0978; observed 139.0974), ThThDP (molecular formula $\text{C}_{12}\text{H}_{18}\text{N}_4\text{O}_8\text{P}_2\text{S}$; calculated $[\text{M}+\text{H}]^+$ of 441.0393; observed 441.0386), ThEthCDP (molecular formula $\text{C}_{12}\text{H}_{20}\text{N}_4\text{O}_9\text{P}_2\text{S}$; calculated $[\text{M}-\text{H}]^-$ of 457.0353; observed 457.0347) and ThFAthDP (molecular formula $\text{C}_{12}\text{H}_{20}\text{N}_4\text{O}_8\text{P}_2\text{S}$; calculated $[\text{M}-\text{H}]^-$ of 441.0404; observed 441.0394) were found in each sample tested.

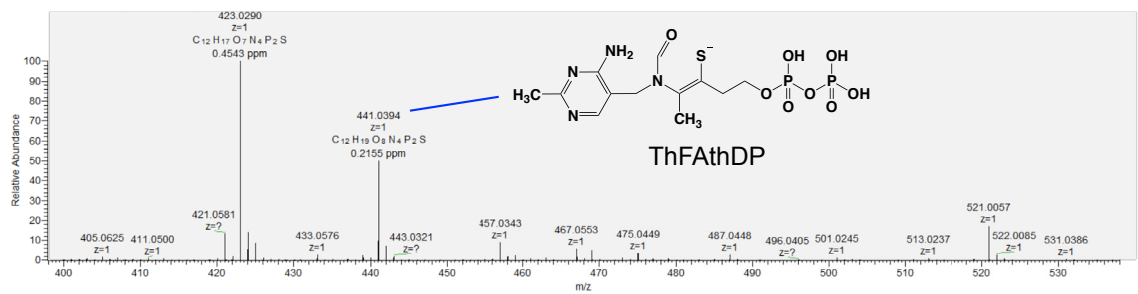
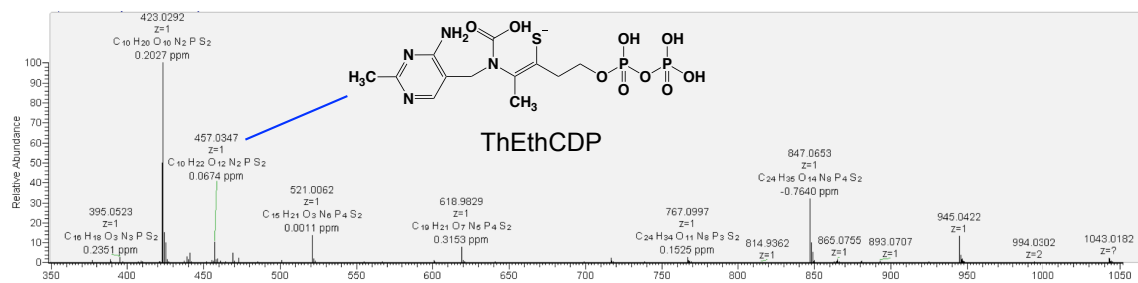
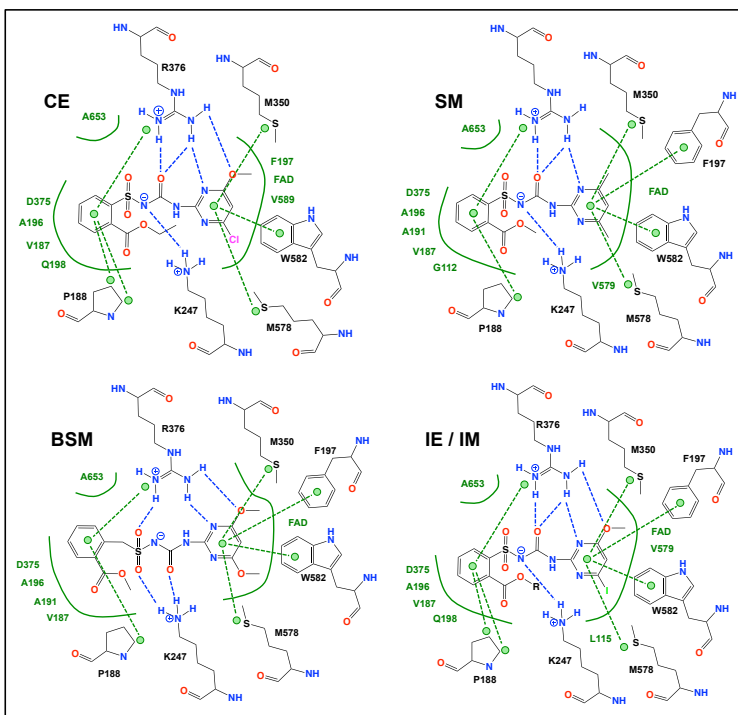
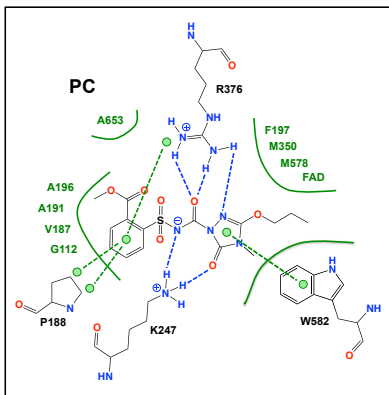
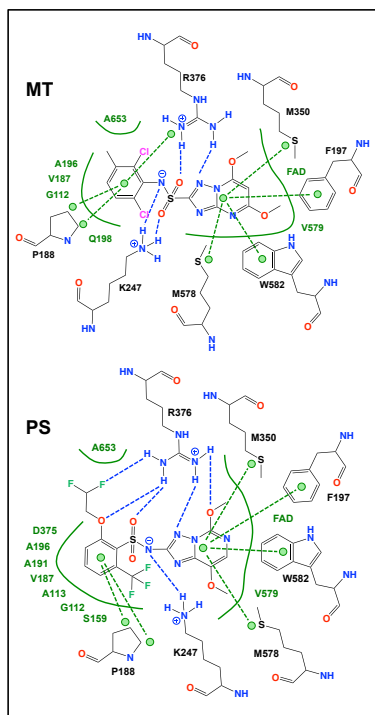


Figure S6 (continued).

Sulfonylureas



Triazolopyrimidines



Sulfonylaminocarbonyl-triazolinone

Figure S7. Contacts of SUs, TPs and SCTs with CaAHAS. Hydrogen bonds are represented with blue broken lines. Van der Waals and hydrophobic interactions are represented with green solid lines. Green circles linked by green broken lines represent a π interaction. Interactions were determined using Arpeggio (4).

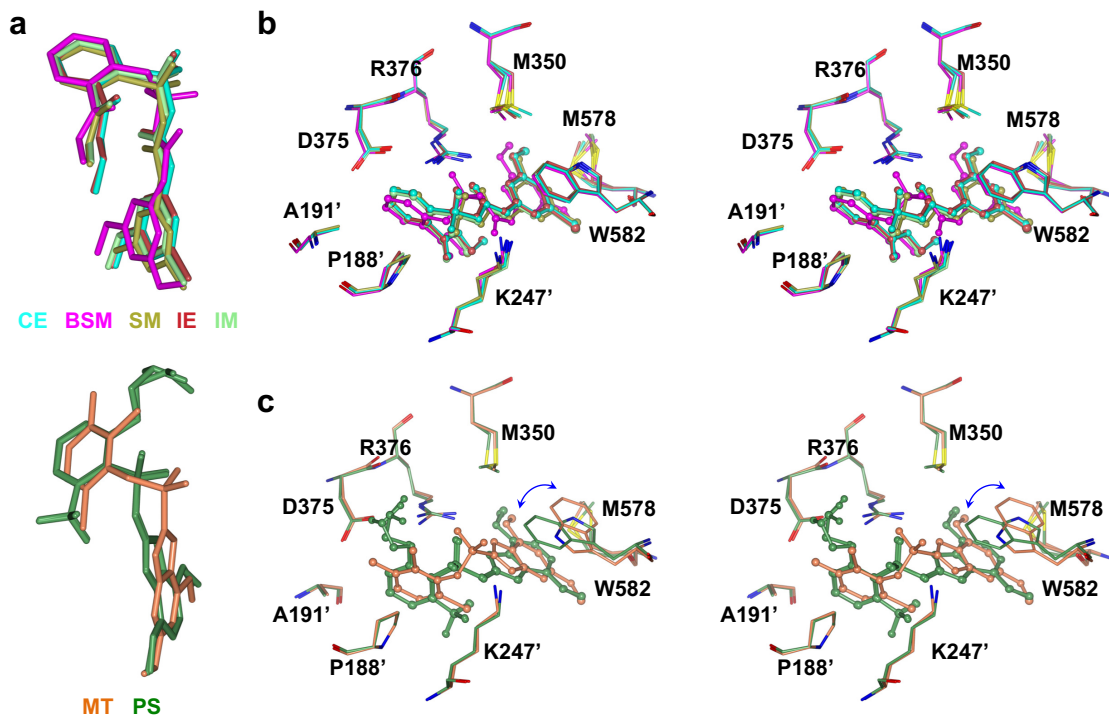


Figure S8. Binding mode of SUs and TPs in CaAHAS. **a** Overlay of the CaAHAS-SU (top) or the CaAHAS-TP (bottom) complexes showing the conformation of each herbicide in their binding site. The inhibitors are coloured cyan (CE), pink (BSM), gold (SM), red (IE), light green (IM), orange (MT) or dark green (PS). **e** Stereoview of the SU binding site in CaAHAS with all five SU complexes superposed. **f** Stereoview of the TP binding site in CaAHAS with the MT and PS complexes superposed. The arrow shows the flexibility of W582 to accommodate either MT or PS in the herbicide-binding site. The herbicides are represented in ball and stick models and the residues in the binding site are depicted as sticks. The colour scheme is as per panel a.

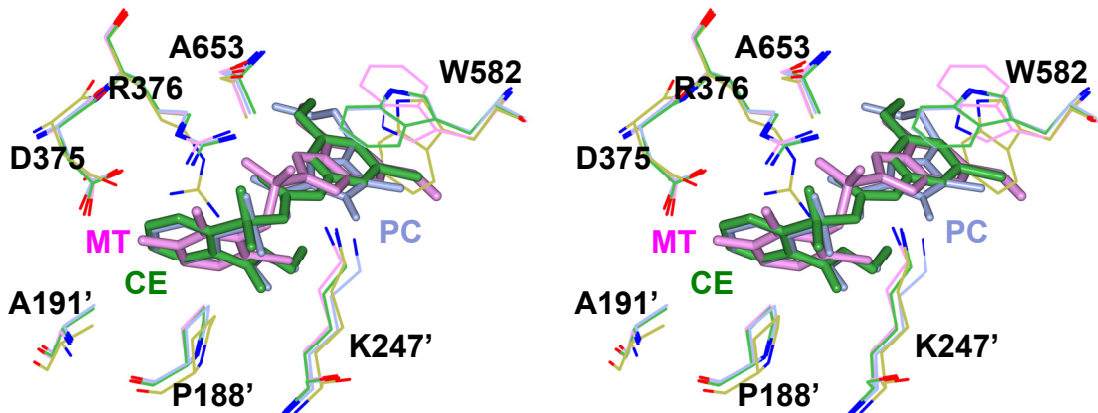


Figure S9. Herbicide binding induces side-chain adjustments to the residues of the CaAHAS herbicide-binding site. Stereoview of the binding mode of three families of herbicides in complex with CaAHAS. Superposition of the CaAHAS-CE, -PC and -MT complexes onto the 3D coordinates for uninhibited CaAHAS show that, upon herbicide binding, a number of side-chain adjustments occur to the residues of the herbicide-binding cavity, depending on the structure of each inhibitor. These adjustments are particularly pronounced for R376 and W582, whose side chain positions in uninhibited CaAHAS block inhibitor binding. The side chains of both residues rotate ~90°, induced by the contacts formed with the herbicides (up to four hydrogen bonds in the case of R376 and a π stacking interaction for W582). The adjustments observed in other residues of the herbicide-binding site are minimal. The herbicides and residues of the herbicide-binding site in CaAHAS are coloured green for CE, a SU; light blue for PC, a SCT; and pink for MT or PS, both members of the TP family. The corresponding amino acids in the uninhibited enzyme structures are coloured gold.

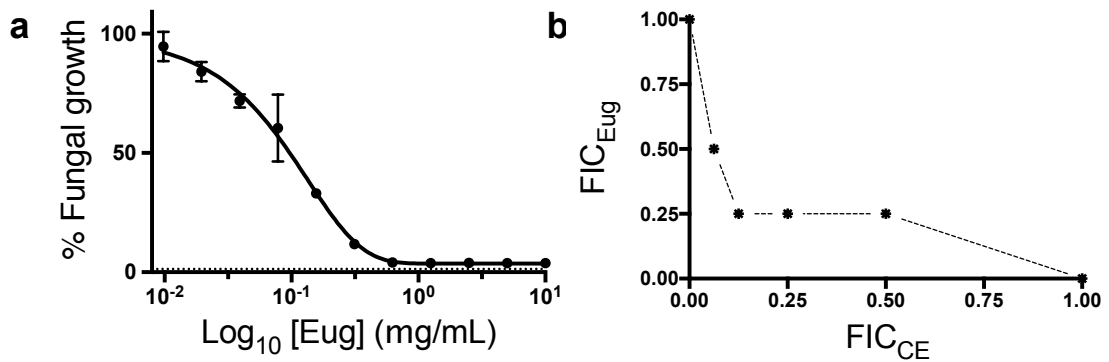


Figure S10. *C. albicans* growth inhibition by eugenol alone and in combination with CE in presence of BCAAs. **a** Antifungal activity of eugenol against *C. albicans* growth in YNB broth supplemented with BCAAs (3.3 mM leucine, 3.3 mM valine and 3.3 mM isoleucine) as sole nitrogen source. 48 h MIC = 0.36 g/mL. Error bars represent the standard deviation of the mean (SEM) ($n = 3$). **b** Isobograms showing the interaction between CE and eugenol against *C. albicans* growth using YNB broth supplemented with BCAAs (as per panel a). The fractional inhibitory concentration (FIC) values for CE (FIC_{CE}) are defined as the MIC of CE in combination with eugenol divided by the MIC of CE alone. The FIC values for eugenol (FIC_{Eug}) were determined in the same way. The concave curve indicates synergism. The FIC index for this drug combination was calculated as $FIC_{CE} + FIC_{Eug} = 0.38$. Eug = eugenol.

Supplementary Tables

Table S1. Data collection and refinement statistics for CaAHAS free enzyme and in complex with commercial herbicides.

	Free	CE	BSM	SM	IE
Crystal parameters					
Unit cell (Å), $a = b, c$	176.04, 177.63	176.31, 177.67	175.41, 177.53	175.89, 177.03	175.33, 176.90
Space group	$P6_222$	$P6_222$	$P6_222$	$P6_222$	$P6_222$
Diffraction data^a					
Temperature (K)	100	100	100	100	100
Resolution range (Å)	49.13-2.97	48.39-2.12	48.21-2.04	48.26-2.15	48.14-1.81
Observations [$I > 0\sigma(I)$]	201,089 (26,091)	1,965,612 (78,872)	2,216,945 (89,435)	951,424 (42,715)	3,185,602 (134,857)
Unique reflections [$I > 0\sigma(I)$]	33,165 (4,342)	91,976 (4,219)	102,110 (4,701)	87,576 (4,151)	145,453 (6,691)
Completeness (%)	97.8 (97.8)	99.7 (93.7)	99.7 (94.3)	99.0 (94.2)	99.7 (94.1)
R_{merge}^b	0.143 (0.792)	0.161 (0.895)	0.129 (0.913)	0.132 (0.650)	0.106 (0.748)
R_{pim}	0.069 (0.385)	0.051 (0.291)	0.040 (0.293)	0.058 (0.290)	0.033 (0.418)
$\langle I \rangle / \langle \sigma(I) \rangle$	9.6 (1.8)	11.3 (2.1)	15.6 (2.6)	10.2 (2.2)	17.6 (1.9)

Refinement statistics					
Resolution limits (Å)	49.13-2.97	46.80-2.12	43.99-2.04	46.65-2.15	46.58-1.80
R_{factor}	0.1533	0.1627	0.1461	0.1445	0.1598
R_{free}	0.1858	0.1871	0.1723	0.1724	0.1763
rmsd ^c bond lengths (Å)	0.003	0.005	0.013	0.003	0.012
rmsd bond angles (°)	0.721	1.058	1.386	0.903	1.430
Ramachandran plot (%)					
Favoured	97.8	98.3	98.3	98.4	98.4
Outliers	0	0	0	0	0

(Table S1 continued)

	IM	PS	MT	PC
Crystal parameters				
Unit cell (Å), $a = b, c$	174.90, 176.93	176.54, 177.79	174.63, 177.39	175.77, 177.34
Space group	$P6_222$	$P6_222$	$P6_222$	$P6_222$
Diffraction data^a				
Temperature (K)	100	100	100	100
Resolution range (Å)	48.06-1.97	48.45-2.13	48.26-2.13	48.27-2.40
Observations [$I > 0\sigma(I)$]	2,455,081 (108,978)	1,952,557 (75,408)	1,912,234 (82,354)	2,761,412 (175,781)
Unique reflections [$I > 0\sigma(I)$]	111,772 (5,263)	91,270 (4,101)	88,099 (4,185)	63,279 (4,339)
Completeness (%)	99.8 (96.3)	99.6 (91.7)	99.7 (94.4)	99.9 (98.5)
R_{merge}^b	0.096 (0.776)	0.187 (0.845)	0.093 (0.817)	0.149 (0.871)
R_{pim}	0.030 (0.245)	0.059 (0.278)	0.029 (0.260)	0.032 (0.317)
$\langle I \rangle / \langle \sigma(I) \rangle$	19.7 (3.2)	10.4 (2.3)	18.7 (2.9)	26.1 (3.0)
Refinement statistics				

	46.55-1.97	44.22-2.13	47.84-2.13	46.69-2.40
Resolution limits (Å)	46.55-1.97	44.22-2.13	47.84-2.13	46.69-2.40
R_{factor}	0.1508	0.1418	0.1482	0.1337
R_{free}	0.1695	0.1609	0.1663	0.1647
rmsd ^c bond lengths (Å)	0.013	0.004	0.005	0.006
rmsd bond angles (°)	1.447	0.907	0.958	0.950
Ramachandran plot (%)				
Favoured	98.7	98.5	98.2	98.4
Outliers	0	0	0	0

^a Values in parenthesis are for the outer-resolution shells: 3.12 – 2.97 Å for the uninhibited enzyme, 2.16 – 2.12 for CE, 2.07 – 2.04 for BSM, 2.19 – 2.15 for SM, 1.84 – 1.81 for IE, 2.00 – 1.97 for IM, 2.16 – 2.13 for PS, 2.16 – 2.13 for MT, and 2.46 – 2.40 for PC. ^b

$R_{\text{merge}} = \sum |I - \langle I \rangle| / \sum \langle I \rangle$, where I is the intensity of an individual measurement of each reflection, and $\langle I \rangle$ is the mean intensity of that reflection. ^c rmsd, root-mean-square deviation.

Table S2. Minimum inhibitory concentrations (MICs) for the AHAS inhibiting commercial herbicides (and controls) against fungal pathogen growth in cell culture.

Candida albicans ATCC 90028 ($\mu\text{g/mL}$)

Inhibitor family	Inhibitor	24 h		48 h		72 h	
		MIC ₅₀	MIC	MIC ₅₀	MIC	MIC ₅₀	MIC
SU	CE	0.03	0.07	0.19	0.35	0.42	0.59
	ES	0.02	0.07	0.21	0.36	0.42	0.64
	BSM	0.03	0.04	0.16	0.29	0.49	1.14
	SM	1.56	3.96	9.30	15.77	16.91	26.55
	CS	5.73	17.14	26.24	52.95	>100	>100
	IE	0.007	0.01	0.03	0.05	0.08	0.18
TP	IM	0.01	0.02	0.05	0.10	0.19	0.31
	PS	1.00	3.75	3.63	6.41	66.32	185.50
	FS	5.92	14.26	25.57	38.74	44.58	87.74
	DS	>100	>100	>100	>100	>100	>100
	CSM	2.02	4.89	>100	>100	>100	>100
	MT	0.24	0.95	1.85	3.10	4.85	8.34
SCT	FT	>100	>100	>100	>100	>100	>100
	PYS	55.08	61.54	>100	>100	>100	>100
	PCS	>100	>100	>100	>100	>100	>100
	TCM	48.59	70.49	>100	>100	>100	>100
	BS	>100	>100	>100	>100	>100	>100
	PTB	>100	>100	>100	>100	>100	>100
IMI	IQ	>100	>100	>100	>100	>100	>100
	IT	>100	>100	>100	>100	>100	>100
Polyene	AMB	0.20	0.28	0.29	0.34	0.32	0.45
Azole	FLU	0.18	0.31	0.30	0.41	0.35	0.60
	ITR	0.02	0.03	0.03	0.04	0.03	0.07

(Table S2 continued)

***Candida glabrata* ATCC 90030 ($\mu\text{g/mL}$)**

(Table S2 continued)

Candida parapsilosis ATCC 22019 (µg/mL)

(Table S2 continued)

***Candida tropicalis* ATCC 750 ($\mu\text{g/mL}$)**

Inhibitor family	Inhibitor	24 h		48 h		72 h	
		MIC_{50}	MIC	MIC_{50}	MIC	MIC_{50}	MIC
SU	CE	0.55	1.45	1.27	2.00	3.01	4.13
	ES	0.19	0.73	6.00	10.04	14.66	22.90
	BSM	0.35	1.16	3.83	6.04	8.00	12.28
	SM	3.33	13.59	>100	>100	>100	>100
	CS	>100	>100	>100	>100	>100	>100
	IE	<0.01	0.03	1.00	1.74	2.94	3.33
TP	IM	<0.01	0.03	0.37	0.77	0.81	2.01
	PS	>100	>100	>100	>100	>100	>100
	FS	43.17	90.50	>100	>100	>100	>100
	DS	>100	>100	>100	>100	>100	>100
	CSM	>100	>100	>100	>100	>100	>100
	MT	3.12	5.23	>100	>100	>100	>100
SCT	FT	>100	>100	>100	>100	>100	>100
	PYS	>100	>100	>100	>100	>100	>100
	PCS	>100	>100	>100	>100	>100	>100
	TCM	>100	>100	>100	>100	>100	>100
	BS	>100	>100	>100	>100	>100	>100
	PTB	>100	>100	>100	>100	>100	>100
IMI	IQ	>100	>100	>100	>100	>100	>100
	IT	>100	>100	>100	>100	>100	>100
Azole	FLU	2.91	6.22	6.11	11.55	12.50	>100

(Table S2 continued)

***Candida krusei* ATCC 6258 (µg/mL)**

Inhibitor family	Inhibitor	24 h		48 h		72 h	
		MIC ₅₀	MIC	MIC ₅₀	MIC	MIC ₅₀	MIC
SU	CE	0.43	1.96	2.67	5.32	8.57	13.46
	ES	1.00	1.65	6.96	17.53	16.90	25.97
	BSM	0.38	0.88	4.35	26.84	>100	>100
	SM	1.46	3.33	>100	>100	>100	>100
	CS	>100	>100	>100	>100	>100	>100
	IE	0.40	1.00	1.80	4.31	4.74	15.39
TP	IM	0.20	2.56	4.10	13.40	>100	>100
	PS	2.27	9.57	>100	>100	>100	>100
	FS	21.49	43.62	59.49	96.26	61.23	98.54
	DS	>100	>100	>100	>100	>100	>100
	CSM	>100	>100	>100	>100	>100	>100
	MT	8.98	20.34	>100	>100	>100	>100
SCT	FT	>100	>100	>100	>100	>100	>100
	PYS	>100	>100	>100	>100	>100	>100
	PCS	>100	>100	>100	>100	>100	>100
	TCM	>100	>100	>100	>100	>100	>100
	BS	>100	>100	>100	>100	>100	>100
	PTB	>100	>100	>100	>100	>100	>100
IMI	IQ	>100	>100	>100	>100	>100	>100
	IT	>100	>100	>100	>100	>100	>100
Azole	FLU	6.42	25.81	33.49	63.40	55.11	86.59
	ITR	0.10	0.20	0.10	0.20	0.10	0.20

(Table S2 continued)

***Cryptococcus neoformans* ATCC 90113 (µg/mL)**

Inhibitor family	Inhibitor	24 h		48 h		72 h	
		MIC ₅₀	MIC	MIC ₅₀	MIC	MIC ₅₀	MIC
SU	CE	2.75	7.98	13.14	20.85	20.60	27.77
	ES	>100	>100	>100	>100	>100	>100
	BSM	>100	>100	>100	>100	>100	>100
	SM	>100	>100	>100	>100	>100	>100
	CS	>100	>100	>100	>100	>100	>100
	IE	1.00	4.15	3.58	22.18	8.12	36.38
TP	IM	2.76	8.00	16.07	34.99	>100	>100
	PS	>100	>100	>100	>100	>100	>100
	FS	22.42	39.99	>100	>100	>100	>100
	DS	54.09	89.90	>100	>100	>100	>100
	CSM	>100	>100	>100	>100	>100	>100
	MT	19.00	35.44	>100	>100	>100	>100
SCT	FT	>100	>100	>100	>100	>100	>100
	PYS	30.58	56.04	58.78	96.00	59.55	98.32
	PCS	>100	>100	>100	>100	>100	>100
	TCM	>100	>100	>100	>100	>100	>100
	BS	>100	>100	>100	>100	>100	>100
	PTB	>100	>100	>100	>100	>100	>100
IMI	IQ	>100	>100	>100	>100	>100	>100
	IT	>100	>100	>100	>100	>100	>100
Azole	FLU	7.63	15.34	11.55	20.42	16.63	33.37
	ITR	0.06	0.2	0.16	0.24	0.19	0.25

(Table S2 continued)

Saccharomyces cerevisiae Σ1278b (µg/mL)

Inhibitor family	Inhibitor	48 h		72 h	
		MIC ₅₀	MIC	MIC ₅₀	MIC
SU	CE	0.008	0.02	0.01	0.02
	ES	0.08	0.29	0.15	0.57
	BSM	0.02	0.05	0.06	0.10
	SM	0.10	0.20	0.58	0.72
	CS	9.05	23.46	26.16	87.92
TP	PS	0.03	0.06	0.06	0.14
	FS	0.05	0.09	0.09	0.18
	DS	0.06	0.08	0.08	0.17
	CSM	0.03	0.04	0.04	0.08
	MT	0.04	0.05	0.05	0.08
SCT	FT	>100	>100	>100	>100
	PYS	22.71	40.21	37.75	67.77
	PCS	20.13	44.17	34.25	75.60
PB	TCM	1.26	2.61	2.60	6.11
	BS	>100	>100	>100	>100
	PTB	>100	>100	>100	>100
IMI	IQ	>100	>100	>100	>100
	IT	>100	>100	>100	>100
Azoles	FLU	10.83	17.03	14.53	23.08
	ITR	1.45	3.33	1.57	3.90

References

1. McCourt JA, Pang SS, King-Scott J, Guddat LW, & Duggleby RG (2006) Herbicide-binding sites revealed in the structure of plant acetohydroxyacid synthase. *Proc. Natl. Acad. Sci. U.S.A.* 103(3):569-573.
2. Krieger E, et al. (2009) Improving physical realism, stereochemistry, and side-chain accuracy in homology modeling: Four approaches that performed well in CASP8. *Proteins* 77(Suppl. 9):114-122.
3. Lonhienne T, et al. (2016) Commercial herbicides can trigger the oxidative inactivation of acetohydroxyacid synthase. *Angew. Chem. Int. Ed. Engl.* 55:4247-4251.
4. Jubb HC, et al. (2017) Arpeggio: a web server for calculating and visualising interatomic interactions in protein structures. *J. Mol. Biol.* 429:365-371.